Journal of Energy Chemistry 57 (2021) 650–655

Contents lists available at ScienceDirect

Journal of Energy Chemistry

journal homepage: www.elsevier.com/locate/jechem

http://www.journals.elsevier.com/journal-of-energy-chemistry/

Achieving long-cycling sodium-ion full cells in ether-based electrolyte with vinylene carbonate additive

Juan Shi [a,b,1], Lina Ding [c,1], Yanhua Wan [a], Liwei Mi [b], Linjie Chen [a], Dan Yang [a], Yuxiong Hu [a], Weihua Chen [a,*]

[a] Green Catalysis Center, and College of Chemistry, Zhengzhou University, Zhengzhou 450001, Henan, China
[b] Henan Key Laboratory of Functional Salt Materials, Center of Advanced Materials Research, Zhongyuan University of Technology, Zhengzhou 450007, Henan, China
[c] College of Pharmacy, Zhengzhou University, Zhengzhou 450001, Henan, China

ARTICLE INFO

Article history:
Received 27 September 2020
Revised 23 October 2020
Accepted 23 October 2020
Available online 6 November 2020

Keywords:
Cathode electrolyte interphase
Sodium-ion batteries
Full cell
Ether-based electrolyte
Vinylene carbonate
DFT calculation

ABSTRACT

Application of sodium-ion batteries is suppressed due to the lack of appropriate electrolytes matching cathode and anode simultaneously. Ether-based electrolytes, preference of anode materials, cannot match with high-potential cathodes failing to apply in full cells. Herein, vinylene carbonate (VC) as an additive into $NaCF_3SO_3$-Diglyme (DGM) could make sodium-ion full cells applicable without pre-activation of cathode and anode. The assembled FeS@C || $Na_3V_2(PO_4)_3$@C full cell with this electrolyte exhibits long term cycling stability and high capacity retention. The deduced reason is additive VC, whose HOMO level value is close to that of DGM, not only change the solvent sheath structure of Na^+, but also is synergistically oxidized with DGM to form integrity and consecutive cathode electrolyte interphase on $Na_3V_2(PO_4)_3$@C cathode, which could effectively improve the oxidative stability of electrolyte and prevent the electrolyte decomposition. This work displays a new way to optimize the sodium-ion full cells easily with bright practical application potential.

1. Introduction

Sodium-ion batteries (SIBs) are considered as one kind of the most promising candidates for large-scale energy storage applications. Their electrode materials have been widely developed in recent years [1–7] in which some materials have demonstrated delightful performance meeting the application requirements in some extent, such as phosphates and prussian blue for cathode materials, and hard carbon and chalcogenides for anode materials [8–15]. However, the wicked compatibility of electrolyte between cathodes and anodes leading to the disappointing performance of the assembled full cells, though it is crucial to the practical application of SIBs.

Up to now, almost all reported cathode materials for Na storage, such as $Na_4Fe_3(PO_4)_2(P_2O_7)$, $Na_2Fe(SO_4)_2$, Na_2FePO_4F, $Na_3V_2(PO_4)_3$, Na_xMnO_2, $NaNi_{1/3}Fe_{1/3}Mn_{1/3}O_2$, $Na_xFeFe(CN)_6$, Na_xTMO_2, $Na_3V_2(PO_4)_2F_3$, $NaVPO_4F$, $Na_3V_2(PO_4)_2O_2F$, are studied in the ester-based electrolytes owing to the higher oxidative stability [10,12,15–23]. While most researches about anode materials, for example, FeS_2, MoS_2, CuS, $CoGa_2S_4$, Ni_3S_4, TiO_2, Bi, P, hard carbon, Na, are investigated in ether-based electrolytes, especially $NaCF_3SO_3$-Diglyme (DGM), due to superior SEI layer, thereby leading to the outstanding rate property and long-term cycle stability (Tables S1 and S2) [6,24–30]. If the outstanding characteristics of anode materials want to be kept, ether-based electrolytes with wide electrochemical stability window, especially oxidation stability, are desired to match cathode simultaneously. And the complex and time-consuming pre-activating of the cathode would be avoided when the high electrochemical stability ester-based electrolytes are employed to assemble full cells.

Introducing additives into electrolyte is an effective and simple way to improve the electrochemical property of electrolytes and electrodes [31–36]. Positive effects of vinyl ethylene carbonate (VEC) and fluoroethylene carbonate (FEC) as additives for Na-metal and hard carbon anodes in carbonate-based electrolytes were identified. Cao et al. pointed out that FEC-derived SEI layers on Na metal and hard carbon anodes are compact and dense which could suppress the decomposition of propylene carbonate (PC) efficiently [37]. Intermetallic alloys, such as Ge, Sb, and Sn, and their composites use FEC as an additive into $NaClO_4$-PC induce to form a robust and thin SEI layer enabling a facile Na-ion transfer. Even though electrolyte additives have a great influence on the electrochemical performance of anode materials, the impact of them on the performance of cathodes is also needed to obtain enough attention. Komaba et al. stated that adding FEC in $NaClO_4$-PC is beneficial to form a stable CEI layer on the surface of $NaNi_{1/2}Mn_{1/2}O_2$,

* Corresponding author.
E-mail address: chenweih@zzu.edu.cn (W. Chen).
[1] These authors contributed equally to this work.

https://doi.org/10.1016/j.jechem.2020.10.047
2095-4956/

which can restrain the oxidation of electrolyte [38]. Lee et al. also proved that, with the presence of DEC and FEC in $NaClO_4$-EC/PC, NaF-lean CEI layers on $Na_4Fe_3(PO_4)_2(P_2O_7)$ were formed, thereby improving the reversibility [39]. Nevertheless, as far as we know, there is not reported work about the effect of additives into ether-based electrolytes for SIBs to improve the compatibility of cathode materials, which would benefit the assembly of full cells without pre-activation.

Herein, ether-based electrolyte (1 M $NaCF_3SO_3$-DGM + 5 wt% VC) with extended electrochemical stability window owing to the additive VC could be successfully employed to FeS@C||$Na_3V_2(PO_4)_3$@C full cells without pre-activation of cathode and anode, respectively. The additive VC can induce to form integrity and consecutive CEI layer on $Na_3V_2(PO_4)_3$@C cathode, leading to the oxidation potential of ether-based electrolyte increased. Therefore, it could match with $Na_3V_2(PO_4)_3$@C cathode. At the same time, it can keep working well with the anode. As a result, the ether-based electrolyte (1 M $NaCF_3SO_3$-DGM + 5 wt% VC) can be applied in full cell delivering capacity retention of 67% after 1000 cycles at 0.5C. Furthermore, this electrolyte can be applied to match other cathode materials.

2. Results and discussion

To obtain an effective electrolyte with suitable voltage window for matching with cathode and anode simultaneously, $NaCF_3SO_3$-DGM electrolytes with additive VC (1 M $NaCF_3SO_3$-DGM + VC) was investigated and displayed in Fig. 1(a). Compared with $NaCF_3SO_3$-DGM whose decomposition potential is 3.60 V (*vs.* Na/Na^+), 1 M $NaCF_3SO_3$-DGM + VC could obtain higher oxidative stability up to about 4.15 V (*vs.* Na/Na^+), showing high electrochemical stability. With varied VC contents from 1% to 20%, the ionic conductivity of electrolytes increases from 3 to 4.8 mS/cm gradually. However, there is little effect of VC content on the decomposition potential of electrolytes, and the decomposition potential of them was all about 4.10 V, which would enable it to meet the voltage requirement of many kind cathode materials for SIBs. Therefore, taken the ionic conductivity (5 wt%, 3.97 mS/cm at room temperature), electrochemical stability window and cost into account, 1 M $NaCF_3SO_3$-DGM with 5 wt% VC (1 M $NaCF_3SO_3$-DGM + 5 wt% VC) is chosen to match with the cathode, and then, test its application in full cells.

When $Na_3V_2(PO_4)_3$@C as the cathode, half cells with 1 M $NaCF_3SO_3$-DGM + 5 wt%VC were assembled. The CV curves (Fig. S2a) represent an obvious sharp oxidation peak at 3.48 V, which implies the extraction of Na^+ from $Na_3V_2(PO_4)_3$@C lattice during the charging process. The two overlapped reduction peaks at about 3.25 and 3.12 V are related to the reduction reaction from V^{4+} to V^{3+}. The split peaks are probably attributed to the Na^+ rearrangement, which is in accordance with the first few discharge profiles (Fig. S2b). With the cycle numbers increased, the lower voltage plateau disappears by degrees and polarization increases significantly (Fig. S3). When varying current densities from 0.1 to 5C (Fig. S4), the average specific capacities of $Na_3V_2(PO_4)_3$@C cathode are 114.6, 88.8, 79.5, 72.6, 65.8, and 53.4 mAh/g at current densities of 0.1, 0.2, 0.5, 1, 2, and 5C, respectively. When the current rate goes back to 0.1C, $Na_3V_2(PO_4)_3$@C cathode can quickly resume the capacity of 109.3 mAh/g. $Na_3V_2(PO_4)_3$@C cathode displays the initial discharge capacity as high as 87.8 mAh/g at 0.5C with the initial coulombic efficiency (ICE) of 95.2%, and retains 76.0 mAh/g after 1000 cycles with the capacity retention of 87% in $NaCF_3SO_3$-DGM with 5 wt% VC, indicating excellent cycling performance (Fig. 1b). Therefore, 1 M $NaCF_3SO_3$-DGM + 5 wt% VC can successfully match with $Na_3V_2(PO_4)_3$@C cathode. While half cells with 1 M $NaCF_3SO_3$-DGM cannot work properly (Fig. S5).

When FeS@C as the anode, the cycle performance of half cells with 1 M $NaCF_3SO_3$-DGM + 5 wt%VC was also investigated. The first discharge profile of FeS@C anode exhibits a potential plateau at 0.6 V, which corresponds to the formation of SEI film and the sodiation process. FeS@C anode delivers the initial charge capacity is 273.7 mAh/g with ICE of 68%. As cycling proceeds, the capacity increases up to 315.5 mAh/g after 500 cycles (Fig. S7). Thus, 1 M $NaCF_3SO_3$-DGM + 5 wt% VC can work well in Na||FeS@C half cells.

To evaluate the application of electrolyte $NaCF_3SO_3$-DGM with 5 wt% VC in full cells of SIBs, full cells with FeS@C as anode, and $Na_3V_2(PO_4)_3$@C as cathode were assembled and tested. The charge–discharge curves of full cell show discharge medium voltage are about 1.9 V (Fig. 1d) and deliver a discharge capacity of 73.9 mAh/g in the first cycle based on the mass of $Na_3V_2(PO_4)_3$@C (Fig. S8) with ICE of 67%. The discharge capacity maintains 49.5 mAh/g after 1000 cycles, corresponding to the capacity retention of 67% (Fig. 1c). Furthermore, the energy density and power density of full cell are calculated based on the total mass of $Na_3V_2(PO_4)_3$@C cathode and FeS@C anode (Fig. S9). It exhibits a high initial energy density of 108.4 Wh/Kg and initial power density of 85.6 W/Kg, and remains 75.8 Wh/Kg and 90.0 W/Kg after 1000 cycles at 0.5C. In reported full cells, either cathode or anode is pre-activated in their favorite electrolyte before the assemble process of full cells, which can improve the performance effectively (Fig. 1e). Whereas in this work the FeS@C|| $Na_3V_2(PO_4)_3$@C full cell is assembled facilely without pre-activation and exhibits long cycle lifespan and low capacity decay per cycle (0.03%). Therefore, the $NaCF_3SO_3$-DGM + 5 wt% VC could be applied to the practical application in full SIBs.

To reveal the reason why $NaCF_3SO_3$-DGM with 5 wt% VC could match with $Na_3V_2(PO_4)_3$@C cathode, the solvated sheath structure of Na^+ in this electrolyte was investigated via FTIR (Fig. 2a) and the corresponding energies were calculated by Density Functional Theory (DFT). FTIR results display a progressive upshift of saturated C–H stretching vibration of DGM (2870 and 2825 cm^{-1}) from the pure DGM to the $NaCF_3SO_3$-DGM based electrolyte, which indicates C–H bond energy of $NaCF_3SO_3$-DGM increase (Fig. S10a). The intensity of these two peaks drops with increasing of added VC implying the weakened Na^+-DGM coordination. The peak located at 1830 cm^{-1} corresponds to C=C stretching vibration in VC and its location maintains no significant change while its strength increases with the VC content (Fig. 2b). The spectra in the C=O stretching region located at 1796 cm^{-1} vary as a function of VC content ranging from 0 to 10 wt% and the peaks shift to the higher wavenumber compared with the pure VC solvent. It indicates that VC is introduced to form Na^+-VC complex, leading to an increase of the C=O bond. Moreover, the broad peak located at 1198 cm^{-1} is the characteristic peak of ether species (C–O–C) (Fig. 2c). Compared with the sole DGM solvent, the energy of C–O–C increase with the addition of sodium salt, demonstrating that the O atom of C–O–C is coordinated with sodium ion to form solvated Na^+. And a clear peak position upshift is noted with the addition of VC. According to the reported literature [51], the peaks located at 1033 cm^{-1} are the SO_3 symmetric stretch (Fig. S10b), indicating the triflate anion is free and cannot form Na^+-triflate ion pairs. All these results indicate that VC participates in the solvation process of Na^+, making the solvent sheath structure of Na^+ changes.

DFT calculations of complex VC-Na^+ and DGM-Na with different structures show that the coordination complex formation process favors less steric effect molecule VC to be involved (Tables S3 and S4). And, VC is prone to form Na^+-DGM-VC complex due to lower ionization energy, leading to the variation of FTIR spectra with the addition of VC. When the solvent molecule DGM coordination replaced by the solvent VC, the energy difference during the process indicates that the six-coordination number complex (DGM(2)-$Na^+(VC)_3$) is more stable (Table S5). Electrochemical

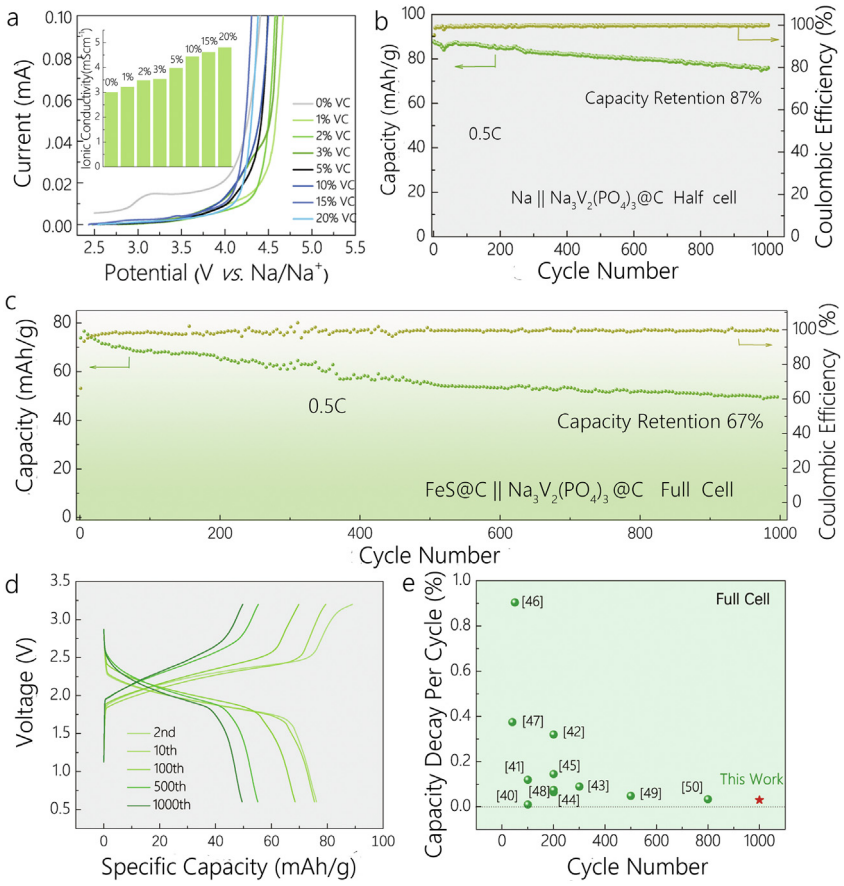

Fig. 1. (a) Ionic conductivity and oxidative stability $NaCF_3SO_3$-DGM and $NaCF_3SO_3$-DGM + 5 wt% VC electrolyte at room temperature; (b) cycle performance of $Na_3V_2(PO_4)_3$@C cathode at 0.5C; (c) cycle performance and (d) charge–discharge profiles of FeS@C||$Na_3V_2(PO_4)_3$@C full cell at 0.5C; (e) the capacity decay per cycle of sodium-ion full cell compared to other literatures [40–50].

stable voltage range of electrolyte are strongly related to two factors. One is the intrinsic oxidation and reduction potential of the electrolyte, which depends on the HOMO/LUMO energy level of ion-solvent complexes. The other is the electrolyte/electrode interface, which is determined by the interface chemistry. Here, the DFT calculations show that the HOMO energy levels of Na^+-DGM-VC complexes are approximate indicating that the added VC cannot improve the intrinsic oxidation potential of the electrolyte (Fig. 2d). Therefore, the electrolyte/electrode interface is the reason why the oxidation potential of electrolyte increased.

Therefore, the morphology and structure of the CEI layer of $Na_3V_2(PO_4)_3$@C electrodes after charging to 3.8 V were measured and displayed in Figs. 3 and S11. TEM images in Fig. 3(a) show that the CEI layer covered on $Na_3V_2(PO_4)_3$@C particle in 1 M $NaCF_3SO_3$-DGM with 5 wt% VC is integrity and consecutive. However, the CEI layer formed in $NaCF_3SO_3$-DGM is non-uniform and un-continuous (Fig. 3b) so that it cannot prevent the further decomposition of electrolyte when the electrode materials are exposed to the electrolyte. Compared the thickness of organic layer and inorganic layer of CEI film induced by two electrolytes, the organic layer in $NaCF_3SO_3$-DGM with 5 wt% VC is thicker than that in no VC-containing $NaCF_3SO_3$-DGM, which is attributed to VC is easy to form poly (vinylene carbonate), as one organic component in the CEI layer.

CEI composition was also investigated via XPS shown in Fig. 3 (c). From the F 1 s spectra of XPS, there are two peaks located at 685.7 eV (Na–F bond), and 688.9 eV (C–F bond), which indicate NaF is an important component of the CEI layer. In C 1 s and O 1 s spectra, Na_2CO_3 and NaOCOR, the oxidation products of VC and DGM, are confirmed to exist on the surface of $Na_3V_2(PO_4)_3$@C electrode. Compared with the CEI formed in 1 M $NaCF_3SO_3$-DGM, the peak intensity of C–O–C and Na_2CO_3 drop, whereas that of C–C=O increases. The results indicate that VC induces to form the CEI layer with less polyether, implying less DGM oxidation. As a result, the CEI layer induced by 1 M $NaCF_3SO_3$-DGM with 5 wt% VC consists of less polyether, more carboxylate, and poly(vinylene carbonate) (Fig. 3d), and the CEI layer is integrity and consecutive which is able to protect the $Na_3V_2(PO_4)_3$@C electrode and prevent the subsequent oxidation of electrolyte.

The possible reactions of VC and DGM molecules during the CEI forming process were derived and shown in Fig. 3(e). DGM molecule generates superoxide and the cyclic carbonate molecule VC is oxidized to peroxyalky carbonates. Under further oxidation, superoxide and peroxyalky carbonates, as intermediate products, decompose to carboxylates, H_2O, and CO_2 which is quickly decomposed to Na_2CO_3, as the inorganic component of the CEI layer. Moreover, VC can polymerize to form poly (vinylene carbonate), which is an organic component of the CEI layer.

To reveal the deep reason why VC-containing electrolyte induces to form integrity and consecutive CEI layer, the HOMO and LUMO energy levels of solvent DGM, and additives VC are investigated via DFT calculation (Fig. 4a). The results show that the difference in HOMO energy level between DGM (−6.51 eV) and VC (−6.95 eV) is small. Therefore, the oxidation potential of the VC molecule is close to that of DGM, thereby leading to synergistic oxidation of VC and DGM. The oxidation products of VC, as

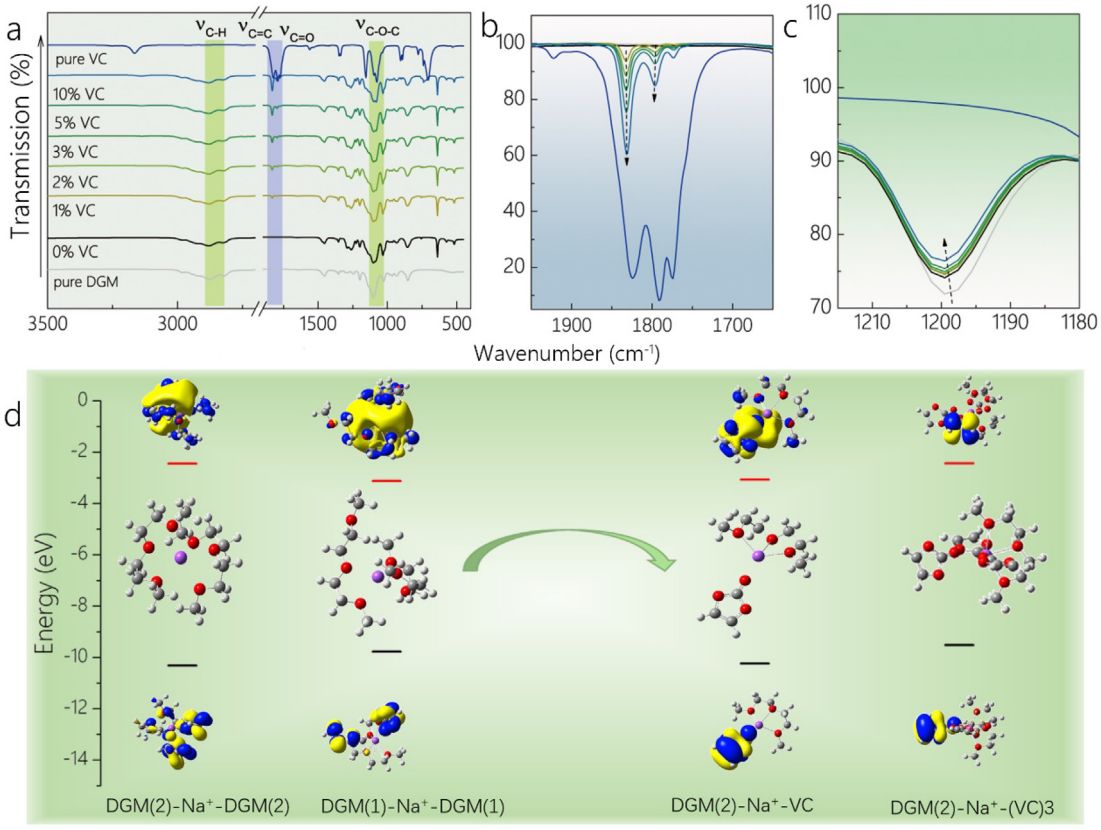

Fig. 2. (a) The whole FTIR spectra of DGM, VC solvent, and $NaCF_3SO_3$-DGM electrolyte with different VC content; the FTIR spectra in the wavenumber range of (b) 2050 cm^{-1}–1650 cm^{-1}, (c) 1215 cm^{-1}–1180 cm^{-1}; (d) the schematic illustration of the change of solvation Na^+ sheath structure with the addition of VC and the energy variation.

some of the components in CEI layer, consist of more organic species, such as poly (vinylene carbonate) and polyester, which is beneficial for the mechanical property of CEI film. Therefore, the synergistic oxidation of VC contributes to forming the integrity CEI layer, enabling to prevent further decomposition of the electrolyte (Fig. 4b).

In addition, according to the DFT calculation, LUMO energy level of VC is lower than that of DGM, so VC has priority over DGM in reduction reaction, thereby VC involved in forming SEI on FeS@C anode. SEM images and XPS spectra of cycled FeS@C anode in 1 M $NaCF_3SO_3$-DGM with 5 wt% VC were also tested to understand the effect of VC on the anode (Fig. S12). The results demonstrate the SEI layers consist of more NaF and Na_2CO_3, which is beneficial to the stability of SEI layer. Therefore, both CEI on cathode and SEI on anode in 1 M $NaCF_3SO_3$-DGM with 5 wt% VC are integrity, which effectively protect the electrolyte from continuous decomposing, thereby ensure the compatibility between them. As a result, the excellent electrochemical performance of the full cell is achieved.

The kinetic property of $Na_3V_2(PO_4)_3$@C cathode cycled in 1 M $NaCF_3SO_3$-DGM with 5 wt% VC is also analyzed. Na^+ diffusion coefficient (D_{Na+}) is calculated according to the EIS spectra of half cells based on $Na_3V_2(PO_4)_3$@C cathode (Fig. S13). It can be obtained that D_{Na+} (5.74×10^{-11} cm^2/s) in the electrode with $NaCF_3SO_3$-DGM + 5 wt% VC is lower than that in $NaCF_3SO_3$-DGM (1.05×10^{-10} cm^2/s). Furthermore, the impedance of CEI layer formed in $NaCF_3SO_3$-DGM + 5 wt% VC is higher than that in $NaCF_3SO_3$-DGM. Therefore, the results indicate the D_{Na+} in the CEI layer is smaller than that of bulk electrode material and at the same time indirectly proves that VC induced integrity CEI layer covers the $Na_3V_2(PO_4)_3$@C cathode entirely.

More importantly, this electrolyte (1 M $NaCF_3SO_3$-DGM with 5 wt% VC) can be applied in other cathode materials, such as $NaFe_{1/3}Ni_{1/3}Mn_{1/3}O_2$ (Fig. S15). The Na||$NaFe_{1/3}Ni_{1/3}Mn_{1/3}O_2$ half cell displays the initial discharge capacity is as high as 101.0 mAh/g at 0.5C with ICE of 91%, and retains 85.3 mAh/g after 50 cycles with the capacity retention of 84% in 1 M $NaCF_3SO_3$-DGM with 5 wt% VC. Therefore, 1 M $NaCF_3SO_3$-DGM with 5 wt% VC has universal applicability in the field of cathode materials of SIBs.

3. Conclusions

In summary, long-life sodium-ion full cells have successfully proceeded in the $NaCF_3SO_3$-DGM electrolyte via the help of VC. Therefore, the effects of VC as an additive in the $NaCF_3SO_3$-DGM electrolyte were identified carefully. The additive VC, of which the HOMO level is close to that of DGM, can be synergistically oxidized with DGM to form an undivided and consecutive CEI layer on $Na_3V_2(PO_4)_3$@C cathode, leading to higher oxidation stability of ether-based electrolyte, which makes $NaCF_3SO_3$-DGM match with $Na_3V_2(PO_4)_3$@C. At the same time, it can keep working well with FeS@C anode. As a result, the $NaCF_3SO_3$-DGM with 5 wt% VC electrolyte can be applied in the FeS@C||$Na_3V_2(PO_4)_3$@C full cells without pre-activation of cathode or anode in their prefer electrolytes, respectively, and delivers excellent cycling performance with the capacity retention of 67% after 1000 cycles at 0.5C. Furthermore, this electrolyte can be applied to match other cathode materials, for example, $NaFe_{1/3}Ni_{1/3}Mn_{1/3}O_2$. This work displays a new way to optimize the full cell of SIBs easily with bright practical application potential.

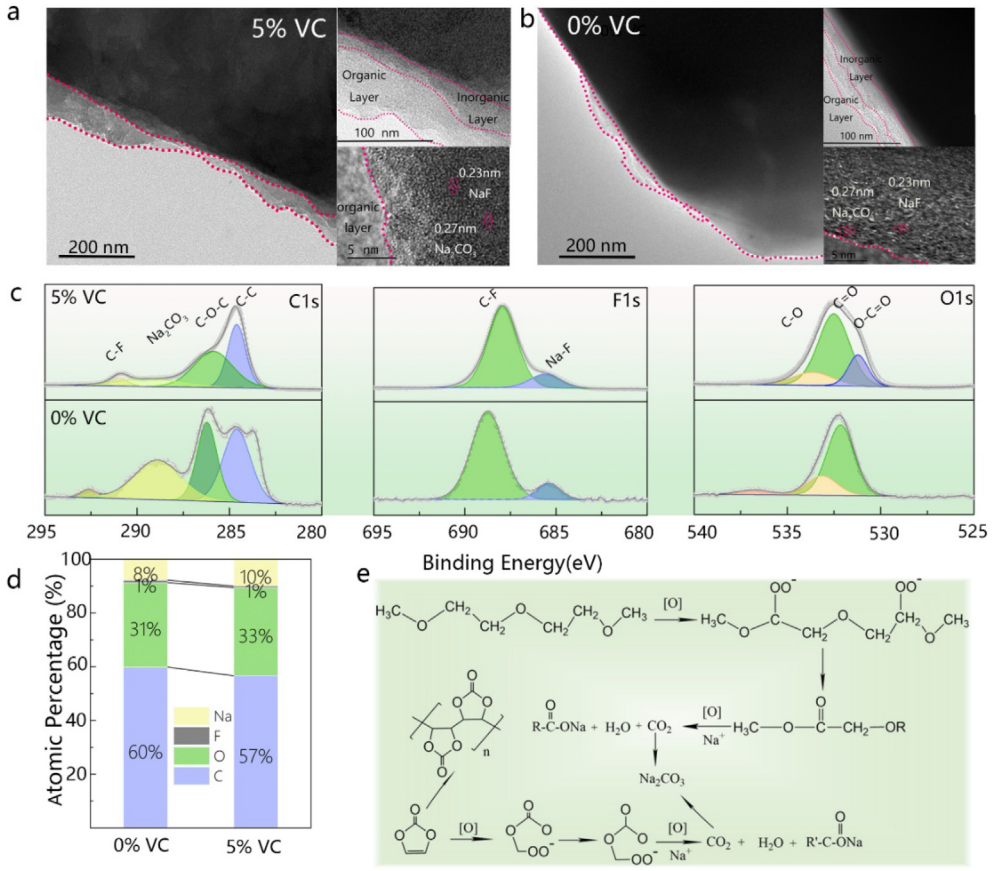

Fig. 3. The TEM images of CEI layer covered on $Na_3V_2(PO_4)_3$@C cathode cycled in (a) 1 M $NaCF_3SO_3$-DGM with 5 wt% VC and (b) $NaCF_3SO_3$-DGM after the first cycle; (c) XPS spectra of CEI layer covered on $Na_3V_2(PO_4)_3$@C cathode cycled in different electrolytes after the first cycle; (d) the atomic percentage of CEI layer in FeS@C|| $Na_3V_2(PO_4)_3$@C full cell with $NaCF_3SO_3$-DGM and $NaCF_3SO_3$-DGM + 5 wt% VC; (e) the possible reaction equation during the oxidation process.

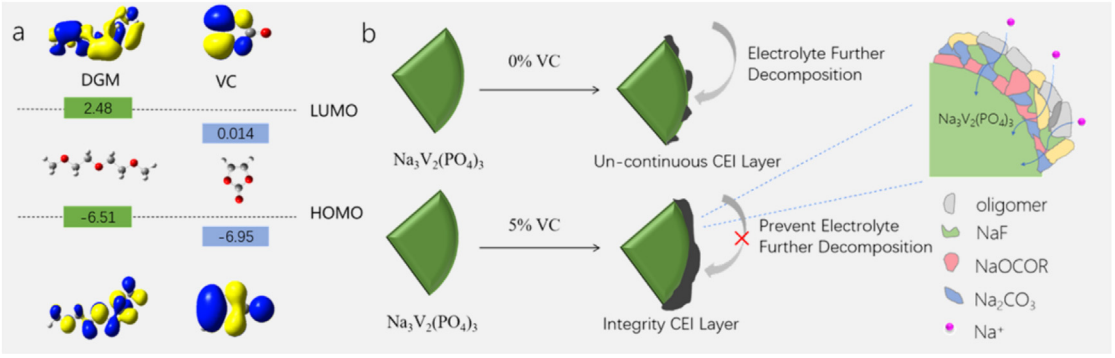

Fig. 4. (a) The HOMO and LUMO energy levels and molecular structure of solvent DGM and additives VC; (b) illustration of the function of VC additives on the surface of $Na_3V_2(PO_4)_3$@C.

Declaration of Competing Interest

The authors declare that they have no known competing financial interests or personal relationships that could have appeared to influence the work reported in this paper.

Acknowledgments

This work was supported by the National Natural Science Foundation of China (Nos. U1804129, 21771164, 21671205, U1804126), Zhongyuan Youth Talent Support Program of Henan Province, Zhengzhou University Youth Innovation Program. And we acknowledge the Zhengzhou University Supercomputing Center for the computational support.

Appendix A. Supplementary data

Supplementary data to this article can be found online at https://doi.org/10.1016/j.jechem.2020.10.047.

References

[1] M. Winter, B. Barnett, K. Xu, Chem. Rev. 118 (2018) 11433–11456.
[2] T. Liu, Y. Zhang, Z. Jiang, X. Zeng, J. Ji, Z. Li, X. Gao, M. Sun, Z. Lin, M. Ling, J. Zheng, C. Liang, Energy Environ. Sci. 12 (2019) 1512–1533.

[3] Y.B. Niu, Y.X. Yin, Y.G. Guo, Small 15 (2019) 1900233.
[4] R. Dunn, H. Kamath, J.M. Tarascon, Science 334 (2011) 928–935.
[5] P.K. Nayak, L. Yang, W. Brehm, P. Adelhelm, Angew. Chem. Int. Ed. 57 (2018) 102–120.
[6] K. Song, C. Liu, L. Mi, S. Chou, W. Chen, C. Shen, Small (2019) 1903194.
[7] L. Chen, K. Song, J. Shi, J. Zhang, L. Mi, W. Chen, C. Liu, C. Shen, Sci. China Mater. (2020), https://doi.org/10.1007/s40843-020-1389-x.
[8] X. Pu, H. Wang, D. Zhao, H. Yang, X. Ai, S. Cao, Z. Chen, Y. Cao, Small (2019) 1805427.
[9] W. Chen, X. Zhang, L. Mi, C. Liu, J. Zhang, S. Cui, X. Feng, Y. Cao, C. Shen, Adv. Mater. (2019) 1806664.
[10] J. Qian, C. Wu, Y. Cao, Z. Ma, Y. Huang, X. Ai, H. Yang, Adv. Energy Mater. (2018) 1702619.
[11] Y. You, A. Manthiram, Adv. Energy Mater. 8 (2018) 1701785.
[12] M. Chen, W. Hua, J. Xiao, D. Cortie, W. Chen, E. Wang, Z. Hu, Q. Gu, X. Wang, S. Indris, S.L. Chou, S.X. Dou, Nat. Commun. 10 (2019) 1480.
[13] T. Wang, K. Yang, J. Shi, S. Zhou, L. Mi, H. Li, W. Chen, J. Energy Chem. 46 (2020) 71–77.
[14] J. Zhang, K. Song, L. Mi, C. Liu, X. Feng, J. Zhang, W. Chen, C. Shen, J. Phys. Chem. Lett. 11 (2020) 1435–1442.
[15] Y. You, S. Xin, H.Y. Asl, W. Li, P.F. Wang, Y.G. Guo, A. Manthiram, Chem 4 (2018) 2124–2139.
[16] P.F. Wang, Y. You, Y.X. Yin, Y.G. Guo, Adv. Energy Mater. 8 (2018) 1701912.
[17] P.F. Wang, H. Xin, T.T. Zuo, Q. Li, X. Yang, Y.X. Yin, X. Gao, X. Yu, Y.G. Guo, Angew. Chem. 130 (2018) 8310–8315.
[18] S. Chen, C. Wu, L. Shen, C. Zhu, Y. Huang, K. Xi, J. Maier, Y. Yu, Adv. Mater. 29 (2017) 1700431.
[19] Z. Gu, J. Guo, Z. Sun, X. Zhao, W. Li, X. Yang, H. Liang, C. Zhao, X. Wu, Sci. Bull. 65 (2020) 702–710.
[20] C. Zhao, J. Guo, Z. Gu, X. Zhao, W. Li, X. Yang, H. Liang, X. Wu, J. Mater. Chem. A 8 (2020) 17454–17462.
[21] X.X. Zhao, Z.Y. Gu, W.H. Li, X. Yang, J.Z. Guo, X.L. Wu, Chem. Eur. J. 26 (2020) 7823–7830.
[22] Y. Yang, W.F. Wei, Rare Met. 39 (2020) 332–334.
[23] G. Yao, X. Zhang, Y. Yan, J. Zhang, K. Song, J. Shi, L. Mi, J. Zheng, X. Feng, W. Chen, J. Energy Chem. 50 (2020) 387–394.
[24] B. Xiao, F.A. Soto, M. Gu, K.S. Han, J. Song, H. Wang, M.H. Engelhard, V. Murugesan, K.T. Mueller, D. Reed, V.L. Sprenkle, P.B. Balbuena, X. Li, Adv. Energy Mater. (2018) 1801441.
[25] Y. Xiao, J.Y. Hwang, I. Belharouak, Y.K. Sun, ACS Energy Lett. 2 (2017) 364–372.
[26] Z. Liu, T. Lu, T. Song, X.Y. Yu, X.W. Lou, U. Paik, Energy Environ. Sci. 10 (2017) 1576–1580.
[27] Y. Fang, L. Xiao, Z. Chen, X. Ai, Y. Cao, H. Yang, Electrochem. Energy Rev. 1 (2018) 294–323.
[28] F. Xie, L. Zhang, C. Ye, M. Jaroniec, S.Z. Qiao, Adv. Mater. (2018) e1800492.
[29] J. Zheng, S. Chen, W. Zhao, J. Song, M.H. Engelhard, J.G. Zhang, ACS Energy Lett. 3 (2018) 315–321.
[30] X.K. Wang, J. Shi, L.W. Mi, Y.P. Zhai, J.Y. Zhang, X.M. Feng, Z.J. Wu, W.H. Chen, Rare Met. 39 (2020) 1053–1062.
[31] A. Ponrouch, E. Marchante, M. Courty, J.M. Tarascon, M.R. Palacín, Energy Environ. Sci. 5 (2012) 8572.
[32] X. Chen, X. Shen, B. Li, H.J. Peng, X.B. Cheng, B.Q. Li, X.Q. Zhang, J.Q. Huang, Q. Zhang, Angew. Chem. Int. Ed. Engl. 57 (2018) 734–737.
[33] G.G. Eshetu, M. Martinez-Ibanez, E. Sanchez-Diez, I. Gracia, C. Li, L.M. Rodriguez-Martinez, T. Rojo, H. Zhang, M. Armand, Chem. Asian J. 13 (2018) 2770–2780.
[34] F. Wu, N. Zhu, Y. Bai, Y. Li, Z. Wang, Q. Ni, H. Wang, C. Wu, Nano Energy 51 (2018) 524–532.
[35] X. Ren, Y. Zhang, M.H. Engelhard, Q. Li, J.G. Zhang, W. Xu, ACS Energy Lett. 3 (2017) 14–19.
[36] J. Zheng, M.H. Engelhard, D. Mei, S. Jiao, B.J. Polzin, J.G. Zhang, W. Xu, Nat. Energy 2 (2017) 17012.
[37] K. Pan, H. Lu, F. Zhong, X. Ai, H. Yang, Y. Cao, ACS Appl. Mater. Interfaces 10 (2018) 39651–39660.
[38] S. Komaba, T. Ishikawa, N. Yabuuchi, W. Murata, A. Ito, Y. Ohsawa, ACS Appl. Mater. Interfaces 3 (2011) 4165–4168.
[39] Y. Lee, J. Lee, H. Kim, K. Kang, N.S. Choi, J. Power Sources 320 (2016) 49–58.
[40] Y. Wang, Y. Wang, W. Kang, D. Cao, C. Li, D. Cao, Z. Kang, D. Sun, R. Wang, Y. Cao, Adv. Sci. 6 (2019) 1801222.
[41] S. Lu, T. Zhu, H. Wu, Y. Wang, J. Li, A. Abdelkader, K. Xi, W. Wang, Y. Li, S. Ding, G. Gao, R.V. Kumar, Nano Energy 59 (2019) 762–772.
[42] J. Tian, J. Li, Y. Zhang, X.Y. Yu, Z. Hong, J. Mater. Chem. A 7 (2019) 21404–21409.
[43] J.H. Jo, J.U. Choi, A. Konarov, H. Yashiro, S. Yuan, L. Shi, Y.K. Sun, S.T. Myung, Adv. Funct. Mater. 28 (2018) 1705968.
[44] Y. Liu, N. Zhang, F. Wang, X. Liu, L. Jiao, L.Z. Fan, Adv. Funct. Mater. (2018) 1801917.
[45] M. Ihsan-Ul-Haq, H. Huang, J. Wu, J. Cui, S. Yao, W.G. Chong, B. Huang, J.K. Kim, Nano Energy 71 (2020) 104613.
[46] C. Dong, L. Guo, H. Li, B. Zhang, X. Gao, F. Tian, Y. Qian, D. Wang, L. Xu, Energy Storage Mater. 25 (2020) 679–686.
[47] Z.H. Zhao, X.D. Hu, H. Wang, M.Y. Ye, Z.Y. Sang, H.M. Ji, X.L. Li, Y. Dai, Nano Energy 48 (2018) 526–535.
[48] M. Sun, Z. Wang, J. Ni, L. Li, Adv. Funct. Mater. 30 (2020) 1910043.
[49] J. Chen, L. Mohrhusen, G. Ali, S. Li, K.Y. Chung, K. Al-Shamery, P.S. Lee, Adv. Funct. Mater. 29 (2019) 1807753.
[50] P. Xue, N. Wang, Z. Fang, Z. Lu, X. Xu, L. Wang, Y. Du, X. Ren, Z. Bai, S. Dou, G. Yu, Nano Lett. 19 (2019) 1998–2004.
[51] J. Wahlers, K.D. Fulfer, D.P. Harding, D.G. Kuroda, R. Kumar, R. Jorn, J. Phys. Chem. C. 120 (2016) 17949–17959.